Chinese Chemical Letters 33 (2022) 4003–4007

Contents lists available at ScienceDirect

Chinese Chemical Letters

journal homepage: www.elsevier.com/locate/cclet

Interface engineering of FeCo LDH@NiCoP nanowire heterostructures for highly efficient and stable overall water splitting

Yong Jiang[1], Yurong Li[1], Yimin Jiang, Xiaorui Liu, Wei Shen, Ming Li, Rongxing He*

College of Chemistry and Chemical Engineering, Southwest University, Chongqing 400715, China

ARTICLE INFO

Article history:
Received 5 October 2021
Revised 26 November 2021
Accepted 29 November 2021
Available online 4 December 2021

Keywords:
OER
Heterostructure
Interface engineering
Water-splitting
DFT

ABSTRACT

Developing efficient and inexpensive OER electrocatalysts is a challenge for overall water splitting. Herein, the heterostructured FeCo LDH@NiCoP/NF nanowire arrays with high performance were rationally designed and prepared using an interface engineering strategy. Benefitting from the special heterostructure between FeCo LDH and NiCoP, the as-synthesized FeCo LDH@NiCoP/NF electrocatalyst exhibits outstanding OER performance with an exceptionally low overpotential of 206 mV to achieve 20 mA/cm^2 current density in an alkaline electrolyte. Importantly, a cell constructed using the FeCo LDH@NiCoP/NF electrocatalyst as cathode and anode just needs a voltage of 1.48 V at 10 mA/cm^2, and shows excellent stability over 80 h. Experimental and theoretical results verified that the introduction of NiCoP efficiently regulates the electronic structure of FeCo LDH, which tremendously boosts the conductivity and intrinsic catalytic activity of FeCo LDH@NiCoP/NF electrocatalyst. The present work provides guidance for the preparation of other efficient and cheap electrocatalytic materials.

Hydrogen production by electrochemical water splitting is a feasible strategy for alleviating the energy crisis and environmental pollution [1,2]. Oxygen evolution reaction (OER) is an important half reaction of water decomposition with a kinetically sluggish four-electron-transfer multi-step process, which severely limits the efficiency of hydrogen production [3]. At present, the state-of-the-art OER catalysts are mainly Ru- and Ir-based materials. However, the scarcity and high cost severely limit their large-scale application. Recently, researchers are committed to developing efficient and low-cost catalysts, for example, metal nitrides [4,5], phosphides [6–8], oxides [1,9,10], sulfides [11,12], hydroxides [13] and (oxy)hydroxides [14,15].

Previous research has identified that the FeCo layered double hydroxides (LDHs) are promising OER catalysts owing to their unique layered structure and tunable compositions [16–18]. However, their electrocatalytic activity is unsatisfactory due to the poor conductivity and intrinsic activity [18–20]. To enhance the electrocatalytic performance of FeCo LDH, many effective methods were developed, for example, doping with other elements to modulate the electronic structure, hybridization with high conductive components to improve electrical conductivity and construction of interface heterostructure to adjust chemical constitutions and crystal structures [21–23]. Among them, heterostructures have attracted great interest for the synergistic effect and electronic structure modulation, which promote interfacial charge transfer and reduce energy barrier of OER process [3,24]. Han *et al.* reported that the electrochemical performance of FeCo LDH for OER can be greatly enhanced by assembling them on reduced graphene oxide with higher conductivity [25]. Gao *et al.* revealed that CoO/CoFe LDHs have high intrinsic catalytic activity and stability, which results from the synergistic effect and strong chemical coupling between CoO and FeCo LDH [26]. Huang *et al.* reported that the hybrid $FeCo_2S_4$@CoFe LDH marerials exhibit excellent electrocatalytic activity, low Tafel slope and high stability because of abundant active sites and efficient electron transfer provided by the special heterostructures [27]. Obviously, the combination of FeCo LDHs and conductive composites to form heterogeneous interfaces with strong electron coupling helps to promote electron transport and improve conductivity. On the other hand, it has been reported that transition metal phosphides (TMPs) exhibit good conductivity and available multiple oxidation states [28]. Especially, for NiCoP, its good conductivity and synergistic effect of Ni and Co make it have outstanding catalytic performance [29]. Furthermore, nickel foam with 3D porous structure can be used as a binder-free electrode, which helps to expose more catalytically active sites and accelerate charge transfer [30,31].

Utilizing the advantages mentioned above, is it possible to design and prepare an efficient and stable electrocata-

* Corresponding author.
E-mail address: herx@swu.edu.cn (R. He).
[1] These authors contributed equally to this work.

https://doi.org/10.1016/j.cclet.2021.11.088
1001-8417/

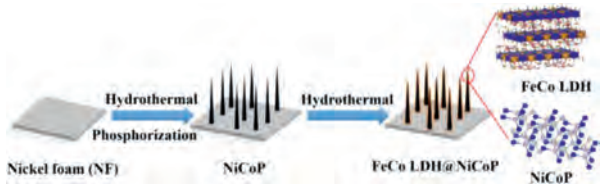

Scheme 1. Schematic diagram of the *in-situ* growth process for FeCo LDH@NiCoP/NF.

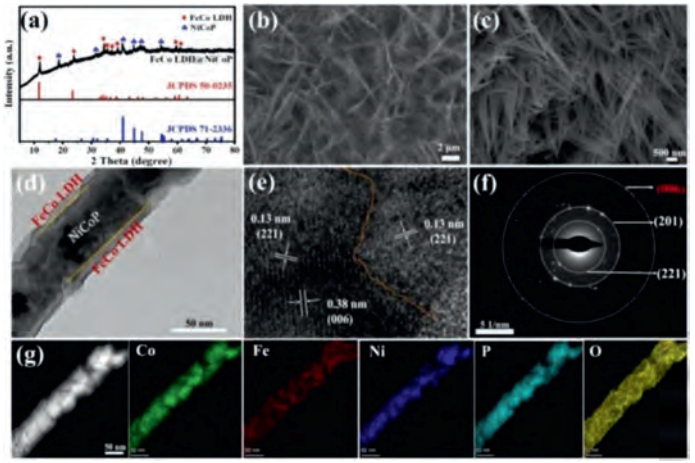

Fig. 1. (a) XRD pattern, (b) SEM image, (c) High-resolution SEM image, (d) TEM image, (e) HRTEM image, (f) SAED interface pattern, and (g) HAADF-STEM image and EDX mapping of the as-prepared FeCo LDH@NiCoP/NF.

lysts? Herein, we designed an ordered 3D FeCo LDH@NiCoP nanowire heterostructure supported *in situ* on Nickel foam (FeCo LDH@NiCoP/NF) through a facile hydrothermal and phosphorization process. As expected, the OER electrocatalyst displays a strong interfacial coupling between FeCo LDH and NiCoP. In addition, compared with Co^{2+}, Co^{3+} with more empty orbitals should lead to the enhancement of electronic acceptance that could be beneficial to absorb OER intermediates. Benefiting from these characteristics, the as-synthesised FeCo LDH@NiCoP/NF possesses an efficient OER activity with an ultra-low overpotential of 206 mV to achieve 20 mA/cm^2 current density and outstanding durability over 95 h. More importantly, the as-prepared catalyst can be assembled into an integral cell for water decomposition with potential merely of 1.48 V to achieved a current density of 10 mA/cm^2 in 1.0 mol/L KOH medium, which outperformed commercial Pt/C||RuO_2 (1.55 V@10 mA/cm^2) and great majority of previous bifunctional catalysts. Experimental and theoretical results demonstrated that the interface engineering to produce heterostructures results in the synergistic effect and electronic modulation of FeCo LDH and NiCoP, and thus promotes the intrinsic catalytic activity and stability of FeCo LDH@NiCoP/NF electrocatalysts.

Scheme 1 illustrated the synthesis process of 3D heterostructured FeCo LDH@NiCoP supported on NF by a simple hydrothermal reaction and phosphating strategy. Such self-assembled *in-situ* 3D array structure on NF generally has good structural stability and excellent conductivity. X-ray diffraction (XRD) peaks of as-synthesized FeCo LDH@NiCoP/NF located at 18.6°, 40.8°, 44.7°, 47.5°, 54.2° are attributed to the (100), (111), (201), (210), (211) planes of NiCoP (JCPDS No. 71-2336), and the peaks centered at 12.0, 23.8, 34.4, 35.5, 37.1, 39.2, 59.6, 60.9° are assigned to the (003), (006), (012), (009), (104), (015), (010), (113) planes of FeCo LDH (JCPDS No. 50-0235), respectively (Fig. 1a and Fig. S1 in Supporting information). These results preliminarily demonstrate the successful preparation of the FeCo LDH@NiCoP/NF heterostructures. In addition, the SEM patterns of FeCo LDH and NiCoP were also measured and the images were shown in Fig. S2 (Supporting information). From Figs. 1b and c, one can find that FeCo LDH@NiCoP/NF maintains the nanowire morphology of the NiCoP precursor after the second hydrothermal reaction, in which FeCo LDH were uniformly grown on NiCoP/NF nanowires to construct the heterostructured FeCo LDH@NiCoP. This 3D heterostructure is conducive to electron transfer, water adsorption and electrolyte diffusion, and exposes more active centers for electrocatalytic process.

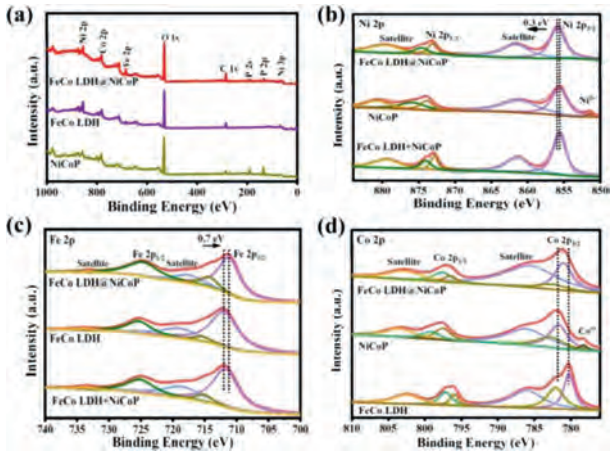

Fig. 2. (a) XPS full spectrum and XPS spectra of (b) Ni 2p, (c) Fe 2p, and (d) Co 2p for FeCo LDH@NiCoP/NF, FeCo LDH/NF and NiCoP/NF, respectively.

Transmission electron microscope (TEM) and high-resolution TEM (HRTEM) were performed to further investigate the microstructure of FeCo LDH@NiCoP/NF and the interfaces between FeCo LDH and NiCoP. As displayed in Fig. 1d, the diameter of FeCo LDH@NiCoP/NF nanowires is about 60–70 nm, and a clear heterojunction interface can be observed in the TEM image. Further, the HRTEM image of FeCo LDH@NiCoP/NF (Fig. 1e) gives the specific interface of FeCo LDH and NiCoP nanowires with lattice distance of 0.13 and 0.38 nm, which are assigned to the (006) planes of FeCo LDH and the (221) planes of NiCoP, respectively. The selected area electron diffraction (SAED) pattern (Fig. 1f) presents a set of distinct rings composed of diffraction spots, corresponding to the (201) and (221) facets of NiCoP and the (006) facet of FeCo LDH, which is consistent with the XRD results (Fig. 1a). These results confirm that the heterogeneous interfaces between FeCo LDH and NiCoP have been constructed successfully.

The TEM-energy dispersive spectroscopy (TEM-EDS) gives the elemental mapping of FeCo LDH@NiCoP/NF and reveals that Co, Fe, Ni, P and O elements are uniformly distributed in heterogenous nanowires (Fig. 1g). From the above results, FeCo LDH was evently grown on NiCoP nanowires to product heterostructures, which provides more active sites and promotes charge transfer between catalyst and electrolyte. The specific surface area of FeCo LDH@NiCoP/NF was characterized by the Brunauer-Emmett-Teller (BET) methods. The N_2 adsorption-desorption isotherms results show that the specific surface area of FeCo LDH@NiCoP/NF (2.343 m^2/g) is larger than that of FeCo LDH (1.418 m^2/g), which is attributed to the formation of heterogeneous structure (Fig. S3 in Supporting information). X-ray photoelectron spectroscopy (XPS) was performed to analyze the chemical composition and valence of the elements for further studying the interfacial effect of heterostructures and clarifying the synergistic effect between NiCoP and FeCo LDH. XPS spectra in Fig. 2a confirmed the presence of Ni, Fe, Co, P and O in FeCoLDH@NiCoP/NF, which is agreement with the elemental mapping analysis.

The Ni 2p spectrum of FeCo LDH@NiCoP/NF shown that the peaks at 855.9, 861.5 and 873.1 eV belong to Ni $2p_{3/2}$, satellite peak and Ni $2p_{1/2}$ (Fig. 2b). Peculiarly, the obvious peak of NiCoP/NF near 852.7 eV corresponds to $Ni^{\delta+}$ (Ni-P), which is unable to observe in FeCo LDH@NiCoP/NF (the possible reason is that FeCo LDH blocks the XPS signal of NiCoP), confirming that NiCoP nanowires are coupled with FeCo LDH nanosheets to form a heterojunction. Note that the binding energy of Ni 2p in FeCo LDH@NiCoP/NF exhibits positive shift by 0.3 eV compared with that in NiCoP/NF, suggesting charge is transferred from NiCoP to FeCo LDH due to the coupling between them [32,33]. This case does not happen in the physical mixture of NiCoP and FeCo LDH. The Fe 2p spectra of FeCo LDH@NiCoP/NF, FeCo LDH/NF, and the mixture of NiCoP/NF and FeCo LDH/NF are given in Fig. 2c. For FeCo LDH@NiCoP/NF, the binding energies at 733.1, 711.2 and 724.6 eV were assigned to the satellite peaks, Fe $2p_{3/2}$ and Fe $2p_{1/2}$, respectively. This indicated that part of the Fe^{2+} ions has been further oxidized during the growth of FeCo LDH [34]. Compared with FeCo LDH, the Fe $2p_{3/2}$ peak of FeCo LDH@NiCoP/NF displays a negative shift of 0.7 eV, which indicates again that charge is transferred from Ni and Fe because of the strong electronic coupling at the heterojunction interface. The Co 2p of FeCo LDH@NiCoP/NF in Fig. 2d shows two fitted peaks at 796.5 and 781.0 eV, which correspond to Co $2p_{1/2}$ and Co $2p_{3/2}$. Peak fitting analysis shows that there are two states of Co for FeCo LDH@NiCoP/NF. The characteristic peaks with binding energies of 782.5 and 797.6 eV are attributed to Co^{2+}, while the peaks at 781.0 and 796.5 eV are assigned to Co^{3+} [35,36]. Similarly, a negative shift in the binding energy of FeCo LDH@NiCoP/NF relative to NiCoP/NF is also observed, which confirms that the existence of strong coupling between FeCo LDH and NiCoP due to the formation of heterostructures. It should also be noted that the Co $2p_{3/2}$ binding energies of pure FeCo LDH/NF and NiCoP/NF are different from that of FeCo LDH@NiCoP/NF, which indirectly proves that FeCo LDH@NiCoP is not a physical mixture of FeCo LDH and NiCoP. As shown in Fig. S4a (Supporting information), the P 2p spectra of NiCoP/NF displays a strong peak at 134.0 eV, which is assigned to the P–O bonds (PO_4^{3-}) [37]. Besides, the binding energy of 129.2 and 129.9 eV are assigned to P^{3-} [38]. Similarly, the XPS peaks of O 1s located at 530.1 and 531.8 eV are attributed to the M-O (M = Ni, Co, Fe) and O–H (Fig. S4b in Supporting information) [39]. Ones can find that the P 2p of FeCo LDH@NiCoP/NF also shifts negative by about 1.0 eV compared with that of NiCoP/NF, which reconfirms the strong electronic coupling between FeCo LDH and NiCoP due to the formation of heterostructured FeCo LDH@NiCoP. This charge transfer generated by electron coupling is very conducive to the reaction kinetics of electrochemical water splitting.

The OER performance of FeCo LDH@NiCoP/NF (loading amount value is $\sim$1.2 mg/cm^2) was tested using a typical three-electrode cell in 1.0 mol/L KOH solution. In addition, the commercial benchmark RuO_2 electrocatalyst, and the prepared FeCo LDH/NF, NiCoP/NF and bare Ni foam were also used for comparison. The activities of the catalysts were estimated by the iR-corrected linear sweep voltammetry (LSV) with a scanning rate of 2 mV/s. As shown in Fig. 3a, FeCo LDH@NiCoP/NF exhibits a superior OER performances with potential of 206 and 258 mV to achieve 20 and 100 mA/cm^2, respectively. Compared with the previous FeCo LDH-based catalysts, the as-synthesised FeCo LDH@NiCoP/NF exhibits a smaller OER overpotential (Table S1 in Supporting information). Tafel slop was used to elucidate the reaction kinetics of water splitting (Fig. 3b). The FeCo LDH@NiCoP/NF catalyst shows ultra-low Tafel slope of 63.6 mV/dec. The low Tafel slop indicates that as-prepared catalyst has a fast kinetic process and remarkable OER activity. The overpotential of FeCo LDH@NiCoP/NF (206 mV) is much lower than those of FeCo LDH/NF (255 mV), NiCoP/NF (256 mV), and bare NF (384 mV) (Fig. 3c). Obviously, the OER performance of FeCo LDH@NiCoP/NF not only far exceeds that of the other samples, even better than that of RuO_2 (292 mV). The significant improvement of the OER activity originates from the strong electronic coupling between FeCo LDH and NiCoP due to the formation of heterostructured FeCo LDH@NiCoP.

The electrochemical active surface area (ECSA) was obtained by double-layer capacitance (C_{dl}) curve method. The obtained C_{dl} value of FeCo LDH@NiCoP/NF is 131.7 mF/cm^2, which is much larger than those of FeCo LDH/NF (4.5 mF/cm^2) and NiCoP/NF (21.9 mF/cm^2), implying that FeCo LDH@NiCoP/NF heterostructure provides more active sites than FeCo LDH/NF and NiCoP/NF (Fig. 3d and Fig. S5 in Supporting information) [40]. Moreover, the electrochemical impedance spectroscopy (EIS) of the catalysts was used to investigate the charge transfer ability between electrolyte and catalyst (Fig. 3e). The FeCo LDH@NiCoP/NF exhibits a smaller charge transfer resistance ($R_{ct} = 0.91\ \Omega$) compared with FeCo LDH/NF (6.44 Ω) and NiCoP/NF (4.73 Ω), indicating that the faster interface electronic transfer and ion diffusion rate, which are conducive to improving the conductivity of catalysts through electron interaction at the heterojunction interface, and thus leads to more superior OER performance for FeCo LDH@NiCoP/NF. The intrinsic OER activity of FeCo LDH@NiCoP/NF and FeCo LDH/NF were also evaluated by measuring the turnover frequency (TOF) at overpotential of 250 and 300 mV (Fig. S6 in Supporting information). The TOF value of FeCo LDH@NiCoP/NF is up to 0.041 and 0.204 s^{-1} at $\eta = 250$ and 300 mV, respectively, which is larger than those of FeCo LDH/NF, again suggesting the superior intrinsic OER performance of FeCo LDH@NiCoP/NF.

Furthermore, the electrochemical OER stability of FeCo LDH@NiCoP/NF was estimated by chronoamperometry measurement. As showed in Fig. 3f, in 1.0 mol/L KOH FeCo LDH@NiCoP/NF has outstanding stability at a low overpotential of 228 mV, because it shows negligible degradation in current density even after continuous operation for 95 h. In addition, the LSV curves of FeCo LDH@NiCoP/NF remain almost unchanged before and after 95 h OER tests (Fig. S7 in Supporting information), further confirming its excellent stability. After long-term OER tests, the structure and composition of FeCo LDH@NiCoP/NF were examined using XRD, SEM and XPS. As demonstrated in Fig. S8a (Supporting information), the XRD pattern manifests that the characteristic peak of FeCo LDH in FeCo LDH@NiCoP/NF decreases, which may be due to the partial transformation of the FeCo LDH phase on the surface of FeCo LDH@NiCoP/NF into the amorphous metal hydroxides (such as FeOOH) under the harsh environment [41]. Meanwhile, the SEM image illustrates that FeCo LDH@NiCoP/NF maintains its original morphology, although some nanowires were slightly agglomerated (Fig. S8b in Supporting information). The XPS measurement shows that after 95 h OER test, the peaks of Fe 2p and Co 2p for FeCo LDH@NiCoP/NF have a slightly negative shifts (Fig. 4a), ascribing to the phase change of part of FeCo LDH on the catalyst surface, which is in line with the XRD result. The peaks centered at 711.7 and 724.3 eV correspond to Fe $2p_{3/2}$ and Fe $2p_{1/2}$ of Fe^{3+} ions, which come from hydroxides produced during the OER process (Fig. 4b) [42]. As shown in Fig. 4c, the peaks at 856.9 and 874.7 eV are ascribed to the oxidized Ni species [43]. Owing to Ni is inside of the heterostructure, the Ni 2p peak does not change significantly before and after OER tests. The binding energy at 796.8 eV is assigned to Co^{3+} of CoOOH (Fig. 4d). Fig. 4e shows a negative shift of binding energy for P 2p, which reveals that the primal metaphosphate P-O species (PO_3^-) are converted to phosphate groups (PO_4^{3-}) [44,45]. The above analyses indicate that metal hydroxides (metals refer to Fe and Co) are formed on the catalyst surface after OER test, which can be confirmed by the great enhancement of the intensity of M-O peaks after and before OER tests (Fig. 4f). Note that the HER activity of FeCo LDH@NiCoP/NF is also excellent, and only an overpotential of 121 mV is required to realize 10 mA/cm^2 current density in alkaline environment

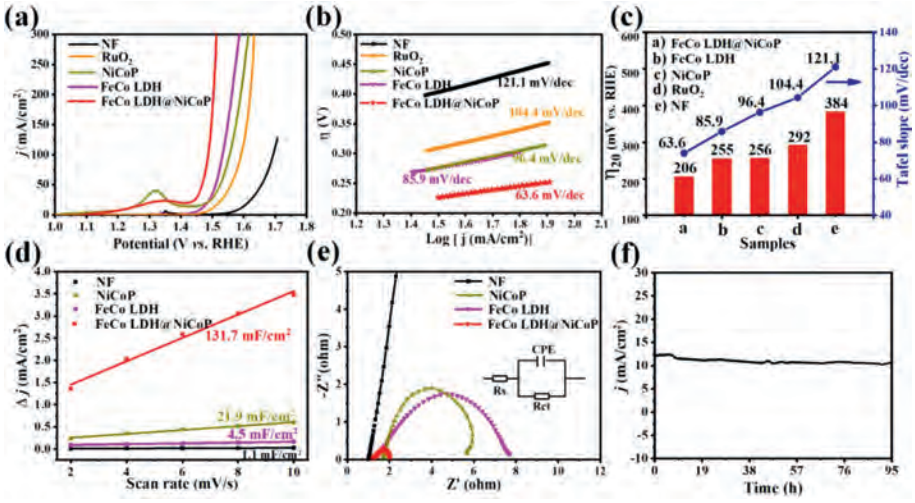

Fig. 3. OER performance of samples in 1.0 mol/L KOH. (a) LSV curves and (b) Tafel plots of the bare NF, RuO_2/NF, NiCoP/NF, FeCo LDH/NF and FeCo LDH@NiCoP/NF. (c) The overpotential at the current density of 20 mA/cm^2 and Tafel value for the corresponding electrocatalysts. (d) C_{dl} of the bare NF, RuO_2/NF, NiCoP/NF, FeCo LDH/NF and FeCo LDH@NiCoP/NF. (e) Nyquist plots at an overpotential of 250 mV. (f) Amperometric *i-t* curve of FeCo LDH@NiCoP/NF.

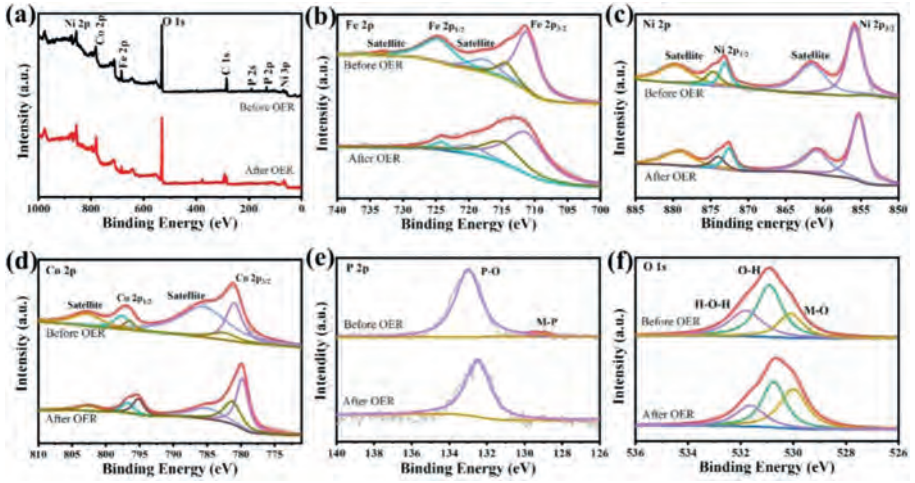

Fig. 4. XPS spectra of FeCo LDH@NiCoP/NF before and after OER tests. (a) XPS full spectrum, (b) Fe 2p, (c) Ni 2p, (d) Co 2p, (e) P 2p, (f) O 1s.

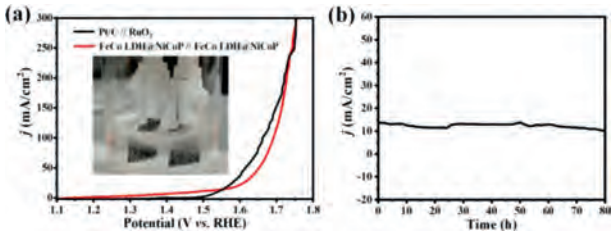

Fig. 5. (a) LSV curve of FeCo LDH@NiCoP/NF||FeCo LDH@NiCoP/NF and Pt/C||RuO_2 in 1.0 mol/L KOH media with a two-electrode system (the scan rate is 2 mV/s). (b) Amperometric *i-t* curve of FeCo LDH@NiCoP/NF.

(Fig. S9 in Supporting information). Considering that iR compensation may affect the performance of the catalyst, the uncompensated polarization curves of all catalysts are also provided (Fig. S10 in Supporting information).

Inspired by the superior OER performance, FeCo LDH@NiCoP/NF can be assembled into a two electrode battery for water decomposition reaction (Fig. 5a). The FeCo LDH@NiCoP/NF||FeCo LDH@NiCoP/NF cell only 1.48 V potential is required to realize 10 mA/cm^2 in alkaline environment, while the commercial Pt/C||RuO_2 cell requires 1.55 V under the same condition (Fig. 5b). The performance of FeCo LDH@NiCoP/NF is superior to that of Pt/C||RuO_2 and most previously reported catalysts (Table S2 in Supporting information). Furthermore, the FeCo LDH@NiCoP/NF||FeCo LDH@NiCoP/NF cell also exhibits outstanding stability (after 80 h of continuous operation at 10 mA/cm^2, the potential change is negligible, Fig. 5b). The gas production rates of cathode and anode were measured by constant current method ($I = 100$ mA/cm^2). The volume of H_2 produced per minute (0.02 mmol) is twice that of O_2 (0.01 mmol). Combined with the atomic ratio of 2:1 in the reaction process, the calculated Faraday efficiencies of the two electrodes are 97% (H_2) and 96.7% (O_2) [46], which further shows that the overall efficiency of the catalyst is high (Fig. S11 in Supporting information).

To deeply understand the nature of FeCo LDH@NiCoP/NF with high OER performance, the DFT calculations were performed. The constructed theoretical models of FeCo LDH, NiCoP and FeCo LDH@NiCoP are illustrated in Fig. 6a and Fig. S12 (Supporting information). Although there are differences between the theoretical model and the real structure of materials, the calculated results are valuable for qualitative understanding of OER performance of FeCo LDH@NiCoP. To clarify the nature of electronic structure regulation in FeCo LDH@NiCoP heterostructures, the work function (Fig. S13 in Supporting information) and the charge density difference (Fig. 6b) between FeCo LDH and NiCoP are calculated.

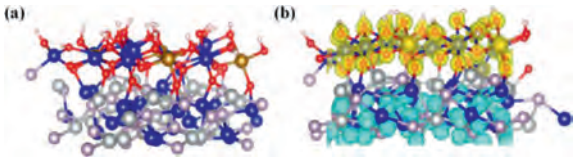

Fig. 6. Schematic model of (a) FeCo LDH@NiCoP heterostructure. (b) The charge density difference for the heterostructure interface of FeCo LDH@NiCoP (the yellow and blue regions indicate the charge accumulation and depletion of the catalyst). The red, pink, gray, dark blue and yellow spheres are, respectively O, P, Ni, Co and Fe atoms, and the isosurface value is 0.271 electron/bohr^3.

The calculated work function of FeCo LDH (006) and NiCoP (111) are 1.66 and 4.89 eV, respectively. The large difference in the work function between the two phases implies that a strong contact potential difference is formed and the strengthened dipole polarization is induced at the FeCo LDH/NiCoP heterointerface, which will lead to the redistribution of interfacial charge. As displayed in Fig. 6b, the charge density on the NiCoP side is lower than that on the FeCo LDH side, indicating that charge redistributes from NiCoP to FeCo LDH, which is also confirmed by the previous XPS results. The calculated results of density of states (Fig. S14 in Supporting information) are also consistent with the analyses of work function and charge density. Consequently, in FeCo LDH@NiCoP, the heterojunction between FeCo LDH and NiCoP leads to strong electronic coupling at the interface and thus produces charge redistribution, which ultimately greatly improves the OER activity of FeCo LDH@NiCoP.

In summary, a novel heterostructured FeCo LDH@NiCoP/NF OER electrocatalyst was successfully fabricated *via* facile hydrothermal and phosphorization process. The experimental results shown that there is a strong interface coupling between FeCo LDH and NiCoP, which accelerates the electron transfer and reaction kinetics. Benefiting from the regulation of interface electronic structure and the improved conductivity brought by heterostructure, FeCo LDH@NiCoP/NF exhibits excellent OER performance with ultra-low overpotential ($\eta_{20} = 206$ mV) and rapid kinetics process with low Tafel slope (63.6 mV/dec), and high durability over 95 h in alkaline environment. Further, the overall water-splitting of FeCo LDH@NiCoP/NF possesses a low overpotential of 1.48 V at 10 mA/cm^2 for more than 80 h under continuous electrolysis, which is better than the recently reported earth-abundant electrocatalysts. Theoretical calculations further explained the outstanding performance of FeCo LDH@NiCoP/NF is originated from the strong electronic coupling between the FeCo LDH/NiCoP interface, which leads to charge redistribution, improved conductivity and enhanced reaction kinetics. Therefore, the strategy of interface engineering herein provides new ways to rationally design various highly efficient water splitting electrocatalysts.

Declaration of competing interest

There are no conflicts to declare.

Acknowledgments

We acknowledge the financial supports from Natural Science Foundation of China (Nos. 91741105, 22006120) and Program for Innovation Team Building at Institutions of Higher Education in Chongqing (No. CXTDX201601011).

Supplementary materials

Supplementary material associated with this article can be found, in the online version, at doi:10.1016/j.cclet.2021.11.088.

References

[1] Z. Xiao, Y. Huang, C. Dong, et al., J. Am. Chem. Soc. 142 (2020) 12087–12095.
[2] S. Sun, X. Zhou, B. Cong, et al., ACS Catal. 10 (2020) 9086–9097.
[3] S.Zhang X.Hu, J. Sun, et al., Nano Energy 56 (2019) 109–117.
[4] J. Jiang, P. Yan, Y. Zhou, et al., Adv. Energy Mater. 10 (2020) 2002214.
[5] H. Yan, Y. Xie, A. Wu, et al., Adv. Mater. 31 (2019) 1901174.
[6] L. Cao, Y. Hu, S. Tang, et al., Adv. Sci. 5 (2018) 1800949.
[7] M. M.Alsabban, X. Yang, W. Wahyudi, et al., ACS Appl. Mater. Interfaces 11 (2019) 20752–20761.
[8] Z. Liang, C. Yang, W. Zhang, et al., Chin. Chem. Lett. 32 (2021) 3241–3244.
[9] L. Zhuang, Y. Jia, H. Liu, et al., Angew. Chem. Int. Ed. 59 (2020) 14664–14670.
[10] X. Yu, Z. Zhao, C. Pei, Chin. Chem. Lett. 32 (2021) 3579–3583.
[11] X. Wang, L. Li, Z. Wang, et al., Electrochim. Acta 353 (2020) 136527.
[12] Y. Li, Q. Guo, Y. Jiang, et al., Chin. Chem. Lett. 32 (2021) 755–760.
[13] Y. Lin, H. Wang, C. Peng, et al., Small 16 (2020) 20024265.
[14] X. Bo, R.K. Hocking, S. Zhou, et al., Energy Environ. Sci. 13 (2020) 4225–4237.
[15] C. Qiang, L. Zhang, H. He, et al., J. Colloid Interface Sci. 604 (2021) 650–659.
[16] J. Zhao, X. Wang, F. Chen, et al., Inorg. Chem. Front. 7 (2020) 737–745.
[17] Y. Yang, W. Zhang, Y. Xiao, et al., Appl. Catal. B: Environ. 242 (2019) 132–139.
[18] R. Yang, Y. Zhou, Y. Xing, et al., Appl. Catal. B: Environ. 253 (2019) 131–139.
[19] S. Liu, J. Zhu, M. Sun, et al., J. Mater. Chem. A 8 (2020) 2490–2497.
[20] L. Yu, H. Zhou, J. Sun, et al., J. Mater. Chem. A 6 (2018) 13619–13623.
[21] J. Han, J. Zhang, T. Wang, et al., ACS Sustain. Chem. Eng. 7 (2019) 13105–13114.
[22] C. Hao, Y. Wu, Y. An, et al., Mater. Today Energy 12 (2019) 453–462.
[23] H. Jia, N. Shang, J. Chen, et al., J. Colloid Interface Sci. 601 (2021) 338–345.
[24] Y. Lin, L. Yang, Y. Zhang, et al., Adv. Energy Mater. 8 (2018) 1703623.
[25] X. Han, C. Yu, J. Yang, et al., Adv. Mater. Interfaces 3 (2016) 1500782.
[26] Z. Gao, T. Ma, X. Chen, et al., Small 14 (2018) 1800195.
[27] Y. Huang, X. Chen, S. Ge, et al., Catal. Sci. Technol. 10 (2020) 1292–1298.
[28] T. Dang, D. Wei, G. Zhang, et al., Electrochim. Acta 341 (2020) 135988.
[29] H.F. Liang, A.N. Gandi, D.H. Anjum, et al., Nano Lett. 16 (2016) 7718–7725.
[30] K.N. Dinh, X. Sun, Z. Dai, et al., Nano Energy 54 (2018) 82–90.
[31] J. Lin, Y. Yan, C. Li, et al., Nano Micro Lett. 11 (2019) 1–11.
[32] Z. Li, W. Niu, L. Zhou, Y. Yang, ACS Energy Lett. 3 (2018) 892–898.
[33] P. Wang, J. Qi, X. Chen, et al., ACS Appl. Mater. Interfaces 12 (2019) 4385–4395.
[34] F. Kong, W. Zhang, L. Sun, et al., ChemSusChem 12 (2019) 3592–3601.
[35] L. Wen, X. Zhang, J. Liu, et al., Small 15 (2019) 1902373.
[36] Y. Zhang, Q. Shao, S. Long, et al., Nano Energy 45 (2018) 448–455.
[37] M. Qu, Y. Jiang, M. Yang, et al., Appl. Catal. B: Environ. 263 (2019) 118324–118333.
[38] W. Li, Y. Jiang, Y. Li, et al., Chem. Eng. J. 425 (2021) 130651.
[39] M. Yang, Y. Jiang, M. Qu, et al., Appl. Catal. B: Environ. 269 (2020) 118803–118812.
[40] S. Trasatti, O.A. Petrii, Pure Appl. Chem. 63 (1991) 711–734.
[41] K. Zhu, X. Zhu, W. Yang, Angew. Chem. Int. Ed. 58 (2019) 1252–1265.
[42] L. Wan, Y. Wang, Y. Zhang, et al., Chem. Eng. J. 415 (2021) 128995.
[43] C.J. Xuan, Z.K. Peng, K.D. Xia, et al., Electrochim. Acta 258 (2017) 423–432.
[44] X. Xu, T. Guo, J. Xia, et al., Chem. Eng. J. 425 (2021) 130514.
[45] J. Ryu, N. Jung, J.H. Jang, et al., ACS Catal. 5 (2015) 4066–4074.
[46] T.Q. Yu, Q.L. Xu, G.F. Qian, et al., ACS Sustain. Chem. Eng. 8 (2020) 17520–17526.